

Facile Formation of 2D-3D Heterojunctions on Perovskite Thin Film Surfaces for Efficient Solar Cells

Qingquan He,[†] Michael Worku,[‡] Liangjin Xu,[†] Chenkun Zhou,[§] Haoran Lin,[†] Alex J. Robb,[†] Kenneth Hanson,[†] Yan Xin,[¶] and Biwu Ma^{,†,‡,§}*

[†]Department of Chemistry and Biochemistry, Florida State University, Tallahassee, FL 32306, USA

[‡]Materials Science and Engineering Program, Florida State University, Tallahassee, FL 32306, USA

[§]Department of Chemical and Biomedical Engineering, FAMU-FSU College of Engineering, Tallahassee, FL 32310, USA

[¶]Condensed Matter Science, National High Magnetic Field Laboratory, Tallahassee, FL 32310, USA

KEYWORDS: Perovskite solar cells, 2D-3D heterojunctions, surface passivation, interface engineering, stability

ABSTRACT: The interfaces between perovskite and charge transport layers greatly impact the device efficiency and stability of perovskite solar cells (PSCs). Inserting an ultrathin wide bandgap layer between perovskite and hole transport layers (HTL) has recently been shown as an effective strategy to enhance device performance. Herein, a small amount of organic halide salt, *N,N'*-dimethylethylene-1,2-diammonium iodide, is used to create 2D-3D heterojunctions on MAPbI₃ thin film surfaces by facile solution processing. The formation of ultrathin wide bandgap 2D perovskite layer on top of 3D MAPbI₃ changes the morphological and photophysical properties of perovskite thin films, effectively reduces the surface defects, and suppresses the charge recombination in the interfaces between perovskite and HTL. As a result, a power conversion efficiency of ~ 20.2%, with an open circuit voltage of 1.14 V, a short-circuit current density of 22.57 mA cm⁻², and a fill factor of 0.78, is achieved for PSCs with enhanced stability.

1. INTRODUCTION

Metal halide perovskites have attracted tremendous attentions as new generation functional materials for a variety of optoelectronic devices, owing to their exceptional optical and electronic properties, as well as low temperature solution processability.¹⁻⁸ Remarkable successes have been achieved for perovskite solar cells (PSCs) during the last decade, with the power conversion efficiency (PCE) improved from 3.8 % in 2009 to nowadays more than 23%, thanks to relentless efforts on materials engineering and device structure optimization.^{1, 5, 7, 9, 10}

Among various approaches to enhancing the device performance of PSCs, surface passivation and interface engineering have been shown to not only significantly increase the PCE, but also the stability.¹¹⁻¹⁴ To achieve effective surface passivation, formation of ultrathin wide bandgap layer on top of light harvesting three-dimensional (3D) perovskites to suppress charge

recommendation in the interfaces between perovskite and charge transport layers is perhaps the most successful strategy established to date.^{5, 13, 15, 16} Different types of materials have been developed to form such a layer, including two-dimensional (2D) perovskites,^{5, 17-22} insulating polymer,²³⁻²⁷ small organic molecule,^{12, 15, 28-30} organic halide salts,^{10, 31-34} etc.^{13, 20, 35, 36}

2D perovskites have attracted great attention for photovoltaic (PV) applications, owing to their relatively high stability.^{19, 37, 38} Recently, creating 2D-3D perovskite heterojunctions on the surfaces of 3D perovskites by cation exchange has been demonstrated as an effective approach to enhancing the performance and stability of PSCs.^{37, 39} For instance, phenethylammonium iodide (PEAI) was employed to fabricate $\text{PEA}_2\text{PbI}_4\text{-MAPbI}_3$ perovskite thin films,²⁰ with which PSCs with PCEs of up to 19.89% were achieved with enhanced device stability.^{39, 40} Other organic cations used to form 2D-3D perovskite heterojunctions include phenylammonium iodide (PAI), phenylmethylammonium iodide (PMAI), n-butylammonium iodide (BAI), *iso*-butylammonium iodide (iBAI), and n-butylammonium bromide (BABr)^{18, 37, 41, 42} The photovoltaic devices with 2D-3D graded structures all showed improved stability as compared to their 3D counterparts.

Despite those remarkable achievements, most of reports are about the monoammonium halide salts on the formation of 2D-3D perovskite thin films. In general, monoammonium cations (1+) intend to form Ruddlesden-Popper phase 2D perovskites.^{43, 44} A disadvantage of these 2D perovskites is the weak interactions between layers caused by van der Waals gaps, which potentially affect the optoelectronic properties and stability of perovskite thin films as well as devices.^{44, 45} The Dion-Jacobson (DJ) phase 2D perovskites can overcome above drawbacks to some extent due to the strengthening effect of hydrogen bonding interactions between diammonium cations and inorganic slabs. Based on previous reports, diamine-based organic ligands (2+) could form DJ phase 2D perovskites.⁴³⁻⁴⁶ However, according to the best of our

knowledge, there is no report on the use of diammonium halide salt to form 2D-3D heterojunctions for efficient PVs. In addition, the surface treating methods reported to date still have many drawbacks, especially the multistep heated procedures. It is therefore of great interest to develop simple methods for surface passivation of metal halide perovskites.³²

Here we report a facile surface functionalization approach to creating 2D-3D heterojunctions on perovskite (MAPbI₃) thin film surfaces by solution processing of isopropanol (IPA) solution containing an diamine halide salt, *N,N'*-dimethylethylene-1,2-diammonium iodide (DMEDAI₂). Detailed structural characterizations and photophysical studies were performed to reveal the formation of an ultrathin 2D perovskite layer on top of 3D MAPbI₃ thin films. The device performance of PSCs is improved from ~ 18.7 % for the control device without surface treatment to ~ 20.2 % for the device with an ultrathin 2D perovskite layer sandwiched between 3D MAPbI₃ perovskite and hole transport *spiro*-OMeTAD layers. The device stability is also improved due to the formation of 2D-3D heterojunctions.

2. RESULTS AND DISCUSSION

The procedure of preparing pristine and DMEDAI₂ treated MAPbI₃ thin films is shown in Figure 1a. Briefly, MAI-PbI₂ precursor solution was firstly deposited on SnO₂/ITO substrate by a two-step sequential spin-coating process. During the second step, chlorobenzene was dropped onto the rotating substrate as antisolvent to assist the formation of perovskite thin films (see Experimental Section for details). For the preparation of DMEDAI₂ treated perovskite thin films, DMEDAI₂ dissolved in IPA with the concentrations of 0 (abbreviated as IPA), 0.25 (0.25-DMEDAI₂), and 0.5 mg mL⁻¹ (0.5-DMEDAI₂) were dropped on the pristine perovskite thin films and stood for 30 sec before spinning. The stand time was optimized and the influence of stand

time on the thin film properties was discussed in the Supporting Information (Figure S1-S3). X-Ray Diffraction (XRD) was used to characterize the obtained pristine and treated perovskite thin films with the results shown in Figure 1b. The diffraction peaks located at about 14.1°, 20.0°, 28.4°, and 31.9° in all patterns are corresponding to the (110), (112), (220), and (222) crystal planes of MAPbI₃ with a tetragonal phase, respectively, suggesting that the DMEDA I₂ treating process occurred on the surface of perovskite thin films and did not destroy MAPbI₃ perovskites underneath.^{11, 47, 48} UV-vis absorption spectra of the obtained perovskite thin films shown in Figure 1c also confirmed the preservation of 3D MAPbI₃ perovskites after the surface treatment. No obvious change of the absorption intensity after treating by IPA and DMEDA I₂ would ensure efficient light absorption of perovskite thin films.

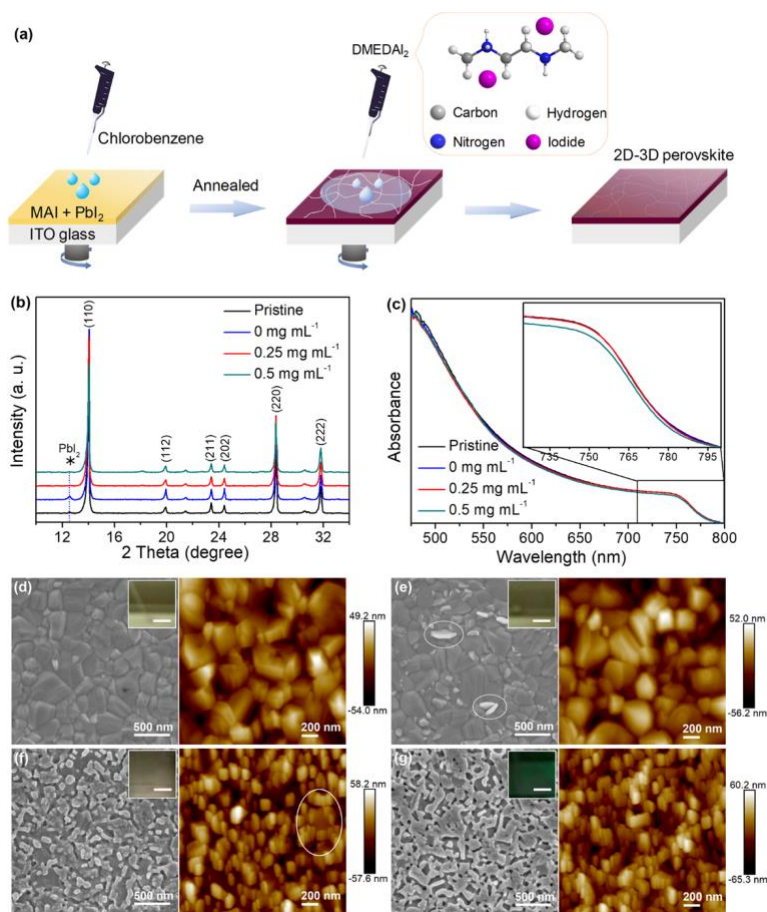


Figure 1. (a) Schematic illustration of the preparation of pristine and DMEDAI₂ treated perovskite thin films. (b) XRD patterns and (c) Uv-vis spectra of MAPbI₃ thin films treated by different concentration of DMEDAI₂. Inset of (c) is a zoom-in view near the absorption edge. Top-view SEM and AFM topographic images of MAPbI₃ treated with different solution: (d) pristine MAPbI₃, (e) 0 mg mL⁻¹ (IPA), (f) 0.25 mg mL⁻¹, and (g) 0.5 mg mL⁻¹. Inset of SEM image highlighted by white square is the corresponding macroscopic digital photograph of perovskite thin films (scale bars, 0.5 cm).

The film morphologies of the perovskite thin films before and after treatment were further characterized by using top-view scanning electron microscope (SEM), and atomic force microscope (AFM) images, as well as the corresponding macroscopic digital photographs, as shown in Figure 1d-g. Crystalline grains with sizes of several hundreds of nanometers can be seen clearly in Figure 1d with the shining surfaces for macroscopic observation. After treating by IPA, some nanosheets with different contrast from the adjacent MAPbI₃ particles appeared within the white oval in Figure 1e. This could be ascribed to the formation of PbI₂ after IPA rinsing, as evident by its characteristic diffraction peak of 12.7° in Figure 1b.^{47, 49, 50} When treated by a 0.25-DMEDAI₂ solution, newly formed nanoparticles covered the surface and grain-boundary of the pristine MAPbI₃ (Figure 1f). The morphology of these new nanoparticles is different from the above-mentioned PbI₂, and the color of treated perovskite thin films slightly changed. By increasing the concentration of DMEDAI₂ solution to 0.5 mg mL⁻¹, the nanoparticles further grew to form condensed coverage on the MAPbI₃ surface, and changed the film color to dark green (Figure 1g), suggesting the formation of more new species on the MAPbI₃ surface.

However, the XRD peaks indexed to the newly formed materials could hardly be distinguished due to the high intensity of MAPbI₃ peaks in Figure 1b. In order to get a better understanding on the newly formed species upon DMEDAI₂ treatment, thinner MAPbI₃ films of about 100 nm (the concentration of perovskite precursor solution was controlled at 0.4 mol L⁻¹) were fabricated and treated under the same conditions to reduce the effect of MAPbI₃ phase and obtain more distinguishable XRD peaks of the new materials (Figure S2a, S4a-b). A series of new periodic peaks located at 13.6°, 18.1°, 22.6°, and 27.2° were observed, which could not be explained by the presence of DMEDAI₂ itself (Figure S4c). Indeed, these new peaks could be indexed as a layer structure stacked parallel to the substrate, suggesting the formation of a 2D perovskite layer on top of 3D MAPbI₃ to create 2D-3D heterojunctions.^{4, 51} The intensity of PbI₂ peak at 12.7° reduced significantly after the DMEDAI₂ treatment, which was likely attributed to the reaction between PbI₂ and DMEDAI₂ at room temperature.⁵² UV-vis absorption spectra of the thinner perovskite films were also recorded and shown in Figure S4d. The absorption edge of pristine 3D MAPbI₃ is 770 nm (bandgap of 1.61 eV). A new peak with the absorption edge of 574 nm could be clearly seen after 0.25-DMEDAI₂ treatment, and the relative peak intensity was enhanced by increasing the concentration of DMEDAI₂ without changing the position. The bandgap of the new formed material is estimated to be around 2.16 eV, which is comparable to those of previously reported 2D perovskite materials.^{4, 17, 45, 53-55}

Fourier-transform infrared (FT-IR) spectra of perovskite powders scraped from the glass substrates were measured to further probe the changes of perovskite thin films after treating by DMEDAI₂ (Figure S5). DMEDAI₂ powder was used as a reference. The peaks around 3170 cm⁻¹ and 3100 cm⁻¹ could be observed in all spectra, which are corresponding to two N-H stretch vibrations in MAPbI₃.^{3, 56, 57} A new peak located at 3033 cm⁻¹ was observed after DMEDAI₂

treating, which is different from that of DMEDAI₂ powder and could be indexed to N-H stretch vibrations of newly formed 2D perovskites. Furthermore, five emerging peaks located from 1350 cm⁻¹ to 750 cm⁻¹ were also detected in DEMDAI₂ treated samples (Figure S5b). The first two peaks have the same locations as those of DMEDAI₂ powder, but the last three peaks located at 1021 cm⁻¹, 857 cm⁻¹, and 755 cm⁻¹ were not observed in spectra of DMEDAI₂ or MAPbI₃, likely correspond to the newly formed 2D perovskites. These results suggested that DMEDAI₂ did not physically attach to the surfaces of MAPbI₃, but underwent cation exchange with MA in 3D MAPbI₃ or reacted with PbI₂ to form 2D perovskites,^{58, 59} which changed the structural and optical properties of the pristine MAPbI₃ thin films.

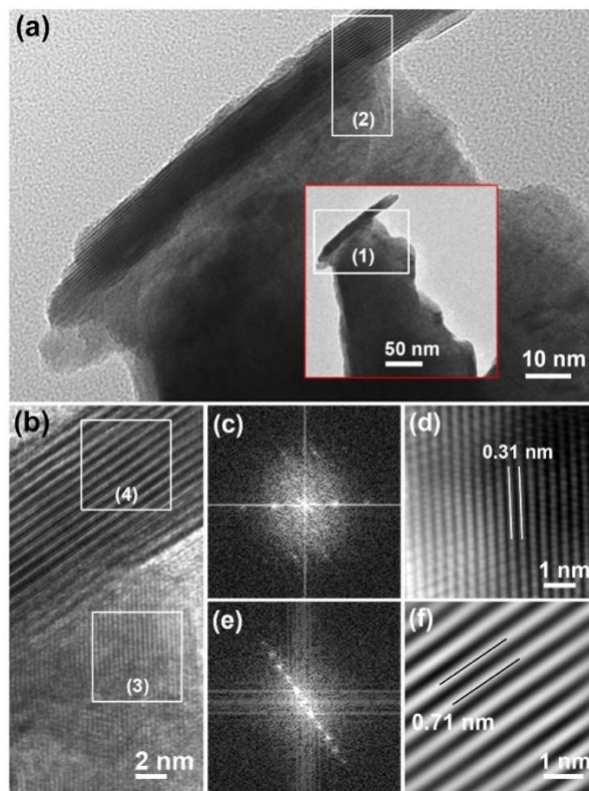


Figure 2. (a) TEM and (b) HRTEM images of MAPbI₃ treated by 0.25-DMEDAI₂ solution. Inset of a demonstrates the low magnification image, and the white rectangle highlighted regions (1)

and (2) were magnified in a and b, respectively. (c, d) and (e, f) demonstrate the Fast Fourier transform (FFT) analysis and simulated HRTEM images of the area of (3) and (4), respectively.

Transmission electron microscope (TEM) and high resolution TEM images of the MAPbI₃ film treated by 0.25-DMEDAI₂ were analyzed to further confirm the formation of 2D-3D heterojunctions, as shown in Figure 2. The inset of Figure 2a is a chunk with the size of several hundred nanometers scratched from 2D-3D perovskite films. In Figure 2a, different contrasts were observed on the heightened region (1), the edge area. By further magnifying the region (2), two distinct areas with “narrow” and “wide” inter-planar spacings can be seen in Figure 2b, which were attributed to two different materials. The HRTEM image of the region (3) was simulated by Fast Fourier transform and shown in Figure 2c-d. An inter-planar spacing of 0.31 nm is well-matched with the (110) reflection of tetragonal 3D MAPbI₃.¹¹ Figure 2f was simulated from the region (4). The inter-planar distance of 0.71 nm could be correlated to a 2D perovskite, which is similar to the (002) reflection (0.80 nm) of 2D PEA₂PbI₄ reported by Yang and coworkers.⁶⁰ The same results were observed in other samples, as shown in Figure S6, confirming the formation of 2D-3D heterojunctions throughout the 3D MAPbI₃ thin film surface by DMEDAI₂ treatment.

Steady-state photoluminescence (PL) spectra of perovskite thin films were recorded to reveal the influences of DMEDAI₂ treatment on the photophysical properties. As shown in Figure 3a, the perovskite thin film treated by 0.25-DMEDAI₂ exhibited higher peak intensity than those of the pristine and pure IPA treated MAPbI₃ thin films, suggesting that the formation of 2D-3D heterojunctions could passivate surface defects and reduce nonradiative recombination.^{29, 61, 62} The decreasing of peak density after treating by a higher concentration DMEDAI₂ (0.5 mg mL⁻¹) could be ascribed to the removal of MAPbI₃ and possible formation of new defects. A small

blue-shift of the PL peaks suggests effective passivation for reducing trap densities near the band edge of DMEDA_I₂ treated perovskite thin films.⁶¹ The broadening of PL peaks was observed in the normalized spectra (Figure S7a), which could be attributed to the formation of 2D-3D heterostructures.^{14, 60} Furthermore, the PL signal belonging to the new formed 2D perovskite can be detected as shown in inset of Figure 3a. The PL peaks centered around 570 nm are observed from the spectrum of DMEDA_I₂ treated samples compared with that of pristine 3D MAPbI₃. These peaks are related to the new formed 2D perovskite on top of 3D MAPbI₃.^{37, 42} The steady-state PL was also performed on back side of the perovskite films (Figure S7b). The only PL peak originated from 3D MAPbI₃ can be observed, indicating that the 2D perovskites only formed on surface of 3D perovskite thin films.

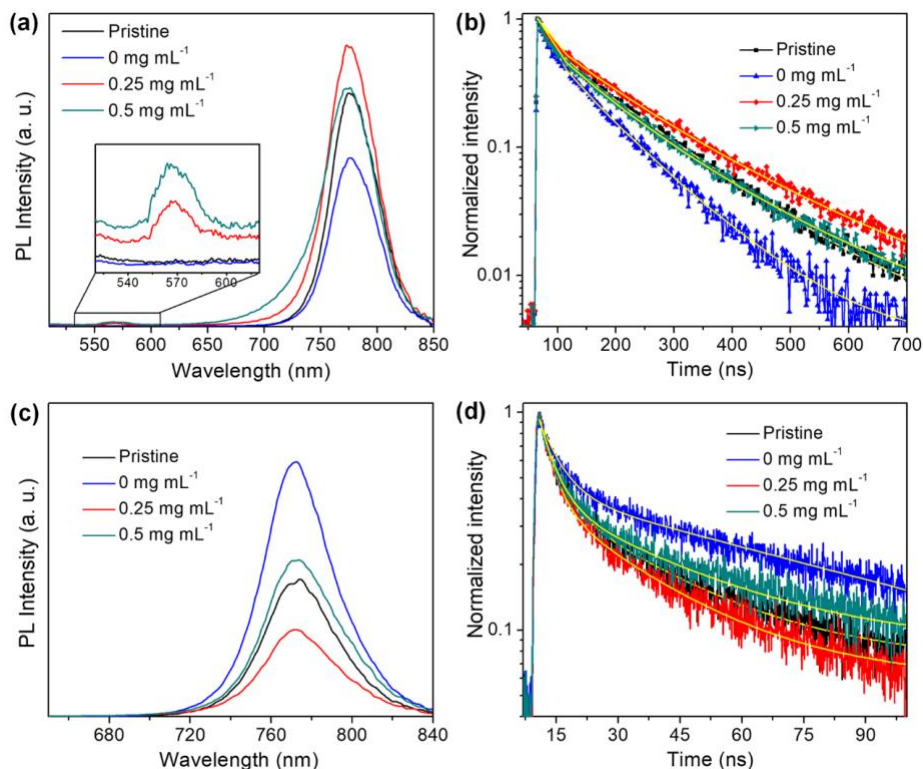


Figure 3. (a) Steady-state and (b) time-resolved PL spectra of the perovskite thin films with and without DMEDA_I₂ treated (architecture: glass/perovskite). Inset of (a) is a zoom-in view near

near 570 nm. (c) Steady-state and (d) time-resolved PL spectra of the perovskite/*spiro*-OMeTAD films (architecture: glass/perovskite/*spiro*-OMeTAD).

The corresponding PL decay lifetimes were investigated by time resolved PL (TRPL) and fitted with bi- (pristine and IPA treated samples) and tri-exponential (DMEDAI₂ passivated 2D-3D samples) equations (Figure 3b and Table S1). The 0.25-DMEDAI₂ treated film displayed a longer average lifetime (168 ns) than those of the pristine MAPbI₃ (136 ns), IPA (99 ns), and 0.5-DMEDAI₂ treated (142 ns) films. The prolonged lifetime of the PL decay supports the reduction of defects on the surfaces.^{14, 61} All these results further confirmed the formation of 2D-3D heterojunctions.

The interfacial charge transfer dynamics between the treated perovskite thin films and hole transport layers (HTLs, *spiro*-OMeTAD) were investigated by steady-state PL and TRPL. The intensity of the PL peak of 0.25-DMEDAI₂ treated perovskite thin film coupled with *spiro*-OMeTAD was the lowest, suggesting that the formation of ultrathin 2D-3D heterojunctions accelerates charge transfer from the perovskite thin films to the HTLs (Figure 3c).^{10, 49, 61} However, the PL peak intensity of DMEDAI₂ (0.5 mg mL⁻¹) treated sample is higher than that of pristine MAPbI₃. This result can be attributed to too thick 2D perovskite was formed on top of 3D MAPbI₃ thin films after treating with higher concentration of DMEDAI₂, affecting the charge transfer between perovskites and HTL. Nevertheless, the trends of changes of PL intensities for glass/perovskite thin films and glass/perovskite/HTL devices are comparable with the increasing of DMEDAI₂ concentration. Figure 3d shows the corresponding TRPL spectra of the perovskite/*spiro*-OMeTAD films. The lifetimes were fitted with bi-exponential model and presented in Table S2. The 0.25-DMEDAI₂ treated perovskite thin film displayed a lifetime of 7.5

ns, which was lower than those of pristine (10.4 ns), IPA (21 ns), and 0.5-DMEDAI₂ treated (13 ns) samples.

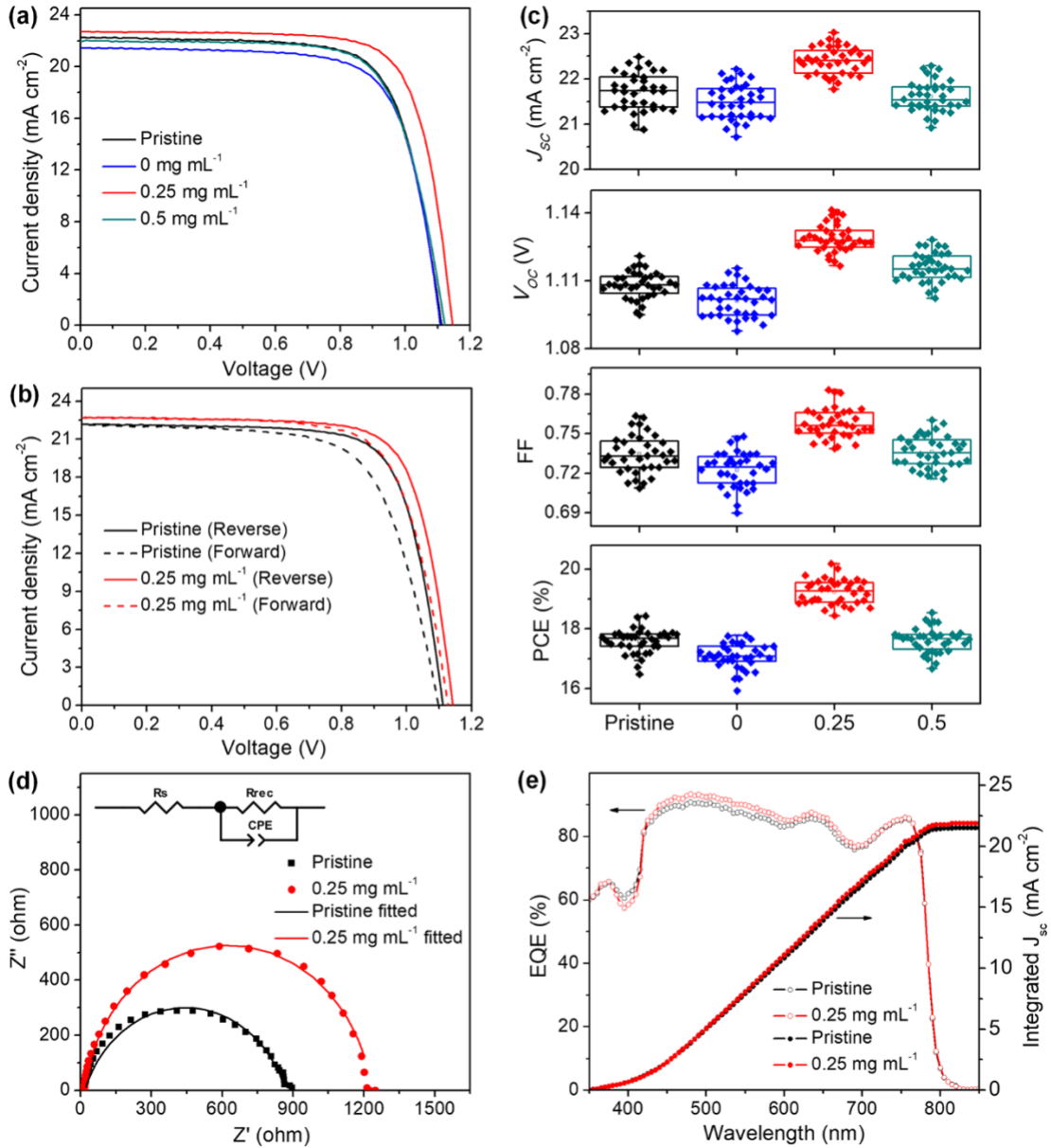


Figure 4. (a) J - V curves of the best-performing devices based on pristine and DMEDA I₂ treated MAPbI₃ thin films. (b) J - V curves of the PSCs measured in different scan directions. (c) Statistical distribution (J_{sc} , V_{oc} , FF, and PCE) of the devices based on different perovskite thin

films (mg mL^{-1}). (d) Nyquist plots of PSCs measured in the dark with a bias of 1.1 V. Inset: the equivalent circuit model. (e) EQE and the corresponding integrated J_{SC} curves of PSCs.

Planar n-i-p PSCs with a device configuration of ITO/SnO₂/perovskite/spiro-OMeTAD/Ag were fabricated and tested to investigate the impact of DMEDAI₂ treatment (Figure S8). The fabrication procedures were kept the same, except varying the perovskite layers. The current density-voltage (J - V) curves for the best performing devices are shown in Figure 4a, and the corresponding photovoltaic characteristics were summarized in Table 1. The PSCs based on pristine MAPbI₃ gave a PCE of 18.7 % with a short-circuit current density (J_{SC}) of 22.14 mA cm^{-2} , an open-circuit voltage (V_{oc}) of 1.11 V, and a fill factor (FF) of 0.76, respectively. The device fabricated with 0.25-DMEDAI₂ treated perovskite exhibited an increased J_{SC} of 22.57 mA cm^{-2} , a V_{oc} of 1.14 V, a FF of 0.78, subsequently an enhanced PCE to 20.2 %. While the devices based on IPA and 0.5-DMEDAI₂ treated perovskite films just gave the PCE of 17.8 % and 18.5 %, respectively. Additionally, PSCs based on thinner perovskite films were fabricated to evaluate the performance of thinner films (about 100 nm) in solar cells. The J - V curves and corresponding photovoltaic parameters are shown in Figure S9 and Table S3, respectively. The changes of V_{oc} , FF, and PCE of PSCs based on these thinner perovskite films are consistent with those of devices based on thicker perovskite films, validating the positive effects of this surface passivation process.

Table 1. Photovoltaic characteristics of the best-performing devices.

Sample	J_{SC} (mA cm^{-2})	V_{oc} (V)	FF	PCE (%)
Pristine	22.14	1.11	0.76	18.69
0 mg mL^{-1}	21.76	1.11	0.74	17.79
0.25 mg mL^{-1}	22.57	1.14	0.78	20.18

0.5 mg mL⁻¹ 22.06 1.12 0.75 18.54

The devices were measured under both forward and reverse scans to evaluate their hysteresis behaviors (Figure 4b and Table S6). The hysteresis index ($H = (PCE_{\text{reverse}} - PCE_{\text{forward}})/PCE_{\text{reverse}}$) was used to determine the degree of hysteresis.⁶³ PSCs based on 2D-3D perovskites showed a lower hysteresis (6%) compared with that of pristine MAPbI₃ (11%). The lower hysteresis of 2D-3D devices can be attributed to the new formed 2D perovskite layer on top of 3D MAPbI₃, which suppresses the migration of iodide ions, and inhibits the ion accumulation at the interfaces between the perovskite and HTL (Spiro-OMeTAD). On the other hand, the formation of 2D-3D perovskites could deactivate the surface traps of 3D perovskite (discussed on PL spectra in Figure 3a) and further improve the hysteresis behavior of PSCs.^{37, 64} To evaluate the reproducibility of the PSCs, more than 30 cells were fabricated and tested for each case with results shown in Figure 4c and Table S4. The devices of pristine MAPbI₃ had an averaged J_{SC} of 21.76 mA cm⁻², V_{OC} of 1.11 V, FF of 0.73, and PCE of 17.6 %, respectively. After treating by 0.25-DMEDA I₂, the parameters were enhanced to an averaged J_{SC} of 22.40 mA cm⁻², V_{OC} of 1.13 V, FF of 0.76, and PCE of 19.2 %, respectively. All the other average photovoltaic characteristics were well-matched with the best performing devices, indicating the reliability of testing results. The improved device performance for PSCs containing ultrathin 2D-3D heterojunctions (0.25-DMEDA I₂) is believed to be a result of reduced nonradiative recombination in the interfaces between perovskite and *spiro*-OMeTAD layers.²⁸

Electrical impedance spectroscopy (EIS) measurement was performed in dark at a bias of 1.1 V to investigate the contact resistance and electron transport properties. Figure 4d displays the Nyquist plots of PSCs with the pristine and 0.25-DMEDA I₂ treated perovskite layer. The inset of Figure

4d is the equivalent circuit model, and the fitted results are presented in Table S5. The series resistance (R_s) correspond to the high-frequency element, and the main arc at the low frequency region is corresponding to the recombination resistance (R_{rec}) at the perovskite/HTL interfaces.^{23, 56, 65} The R_{rec} value of the PSC based on 0.25-DMEDAI₂ treated perovskite thin film (1215 Ω) is higher than that of pristine MAPbI₃ (839 Ω). These results, in agreement with the PL quenching results described in Figure 3c, clearly show that the formation of 2D-3D heterojunctions effectively reduced electron-hole recombination at the perovskite/HTL interfaces, thus improved the V_{oc} and FF in PSCs.⁶⁶ External quantum efficiency (EQE) was measured and shown in Figure 4e to confirm the photocurrents of the $J-V$ scans. The integrated J_{SC} of the device containing 2D-3D heterojunctions is 21.86 mA cm⁻². This is higher than that of pristine MAPbI₃ device (21.45 mA cm⁻²). The result well-matched with the J_{SC} value derived from the $J-V$ measurement (about 3%).

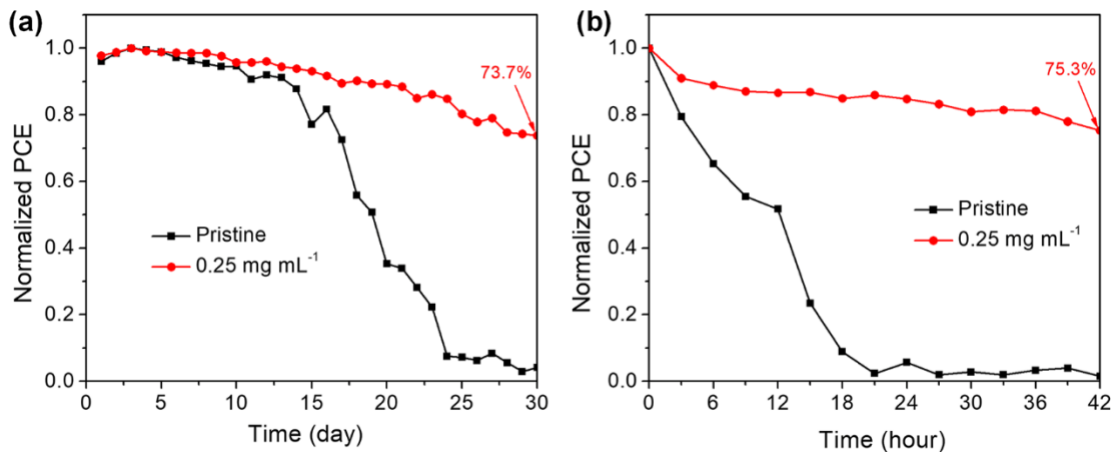


Figure 5. (a) The moisture stability of unencapsulated PSCs stored in ambient conditions (60%-80% relative humidity at room temperature under ambient air). (b) The operational stability of unencapsulated devices under continuous AM 1.5G illumination (60% relative humidity at 40 °C under ambient air).

The unencapsulated PSCs based on pristine and 2D-3D (0.25-DMEDAI₂) containing perovskite thin films were systematically examined to better understand their stability. These devices were stored under ambient conditions with humidity of 60%-80% at room temperature to evaluate the long-term stability. Figure 5a shows the changes of PCEs of the devices in 30 days. The 2D-3D heterojunctions containing PSCs maintained 73.7 % of its initial efficiency, while the MAPbI₃ device completely degraded. The stability of unencapsulated devices under continuous illumination were tested with AM 1.5G in ambient environment (relative humidity of 60%, 40 °C). As shown in Figure 5b and Figure S10, the DMEDAI₂ treated device maintains over 75.3% of its initial PCE after 42 hours of illumination, which is much better than that of pristine MAPbI₃. These results suggested that the stability of PSCs can be enhanced by introducing an ultrathin 2D perovskite layer on top of a 3D perovskite thin film.

3. CONCLUSION

In conclusion, we have developed a facile and effective method for surface modification of perovskite thin films by using a simple organic halide salt DMEDAI₂. The formation of 2D-3D heterojunctions after treating by 0.25 mg mL⁻¹ of DMEDAI₂ can effectively reduce the surface defects and suppress the charge recombination in the interfaces between the photoactive 3D perovskite and hole transport *spiro*-OMeTAD layers in planar PCSs. As a result, an enhanced PCE of ~ 20.2 % was achieved and device stability was also significantly improved. Our simple approach of surface functionalization shows once again the importance of interface engineering to enhance the performance of perovskite solar cells towards their thermodynamic limits, which could also be useful for other optoelectronic devices based on metal halide perovskites.

4. EXPERIMENTAL SECTION

4.1. Materials. Lead iodide was purchased from TCI Chemicals. Methylammonium iodide (MAI), 2,2',7,7'-tetrakis(*N,N*-di-*p*-methoxyphenylamine)-9,9-spirobifluorene (Spiro-MeOTAD), bis(trifluoromethane)sulfonimide lithium salt (Li-TFSI), 4-*tert*-butylpyridine (t-BP), tin (II) chloride (SnCl₂), thiourea (CH₄N₂S), *N,N'*-dimethylethylenediamine (DMEDA), dimethylformamide (DMF), and dimethyl sulfoxide (DMSO) were purchased from Sigma-Aldrich. Tris(2-(1H-pyrazol-1-yl)-4-*tert*-butylpyridine) cobalt (III) tri[bis(trifluoromethane)sulfonimide] (FK-209) was purchased Xi'an Polymer Light Technology Corp. All reagents and solvents were used without further purification unless otherwise stated. Prepatterned ITO-coated glass substrates (20 Ω sq⁻¹) were purchased from Thin Film Devices Inc.

4.2. Synthesis of DMEDA₂I₂. For the synthesis of *N,N'*-Dimethylethylene-1,2-diammonium iodide (DMEDA₂I₂) salts, hydriodic acid solution (2.2 equiv.) and *N,N'*-dimethylethylenediamine (1 equiv.) were added into a solvent of ethanol at 0 °C. After the reaction finished, the organic salts could be obtained after removing solvents and starting reagents under vacuum, followed by washing with ethyl ether for several times. The salts were dried at vacuum oven and kept in a desiccator for use.

4.3. Planar n-i-p perovskite solar cells fabrication. The ITO substrates were sequentially cleaned with sonication in detergent, deionized water, acetone, and isopropanol (IPA) for 25 min, respectively. After drying by nitrogen blow, the cleaned substrates were further treated by UV-ozone for 15 min before deposition of SnO₂ electron transporting layer (ETL). The colloidal SnO₂ quantum dots (QDs) solution was prepared according to previous report with a slightly modified and used for all PSCs in this work.⁶⁷ Briefly, SnCl₂ (284 mg) and CH₄N₂S (112 mg) were dissolved in deionized water (10 mL) in an open vial under magnetic stirring at room temperature for 36 h. The SnO₂ ETL was deposited by spin-coating the filtered (0.45 μm PVDF) SnO₂ QD solution on

cleaned ITO substrate at 3000 rpm for 30 sec and annealed on hot plate at 200 °C for 1 h in air. The ITO/SnO₂ substrate was treated by UV-ozone for 15 min before depositing perovskite layer in glovebox.

The perovskite solution was prepared by dissolving MAI (1.3 mmol) and PbI₂ (1.3 mmol) in DMF/DMSO (1 mL, 4:1 by vol/vol) mixed solvent and stirring at 60 °C for 1 h. For preparing MAPbI₃ film, the solution was deposited on ITO/SnO₂ substrate by two consecutive spin-coating steps of 750 rpm and 4000 rpm for 3 s and 20 s, respectively. During the second step, 180 μ L of chlorobenzene was dropped onto the substrate after 10 s. After all samples finished, the intermediate phase film was annealed on a hotplate at 100 °C for 10 min and cooled down to room temperature. The original perovskite solution was diluted to 0.4 mol L⁻¹ to prepare thinner MAPbI₃ films (about 100 nm, measured by Dektak 150 profilometer). For the preparation of DMEDA I₂ treated perovskite films, the DMEDA I₂ was firstly dissolved in IPA with different concentration including 0 mg mL⁻¹ (IPA), 0.25 mg mL⁻¹ (0.25-DMEDA I₂), and 0.5 mg mL⁻¹ (0.5-DMEDA I₂). The solutions were filtered with 0.2 μ m PTFE and employed to treat the obtained MAPbI₃ film *via* a dropping-standing-spinning procedure. Briefly, 180 μ L of DMEDA I₂ solution was dropped on the ITO/SnO₂/MAPbI₃ substrate and stand for 30 sec before spinning at 3000 rpm for 30 sec. Then, 30 μ L *spiro*-OMeTAD solution containing 50 mg *spiro*-OMeTAD, 18 μ L 4-tert-butylpyridine (*t*-BP), 10 μ L Li-TFSI solution (517 mg/mL in acetonitrile), 4 μ L FK-209 (375 mg/mL in acetonitrile), and 0.5 mL CB was spin-coated onto the perovskite layer at 4000 rpm for 20 s as the hole-transport layer.⁶⁸ Finally, a thickness of 120 nm Ag was deposited by thermal evaporation.

4.4. Characterization. Perovskite films were coated on ITO/SnO₂ substrates for the measurements unless otherwise stated. X-Ray diffraction (XRD) of pristine and DMEDA I₂ treated

perovskite films was performed on a Panalytical X'PERT Pro powder X-ray diffractometer with Cu K α radiation. Uv-vis absorption spectra of films on the glasses were recorded by CARY 5000 UV-Vis NIR spectrophotometer (Agilent Technologies). Surface and cross-sectional morphology of and PSCs were investigated by FEI Nova NanoSEM 400 scanning electron microscope (SEM). Atomic force microscope (AFM) topographic was taken with a Bruker Icon scanning probe microscope in tapping-mode. High resolution transmission electron microscope (HRTEM) images of perovskites were characterized by JEM-ARM200CF (JEOL). The perovskite film was scraped from glass substrate to prepare the samples for TEM characterization. Fourier-transform infrared (FT-IR) spectra of perovskite powder which scraped thinner perovskite film from glass substrates were recorded by PerkinElmer Spectrum 100 FT-IR Spectrometers. Steady-state photoluminescence (PL) and time-resolved PL spectra of pristine and DMEDAI₂ treated perovskite films (architecture: glass/perovskite) and devices (architecture: glass/perovskite/spiro-OMeTAD) were measured at room temperature on a FS5 spectrofluorometer (Edinburgh Instruments). The carrier lifetimes were fitted with a biexponential function $y = A_1 \times \exp(-x/\tau_1) + A_2 \times \exp(-x/\tau_2) + y_0$ or tri-exponential $y = A_1 \times \exp(-x/\tau_1) + A_2 \times \exp(-x/\tau_2) + A_3 \times \exp(-x/\tau_3) + y_0$, and a weighted average lifetime calculated using $\langle \tau \rangle = \sum A_i \tau_i^2 / \sum A_i \tau_i$.

Current density-voltage (J-V) curves of the solar cells were recorded on the IV5 Solar Cell I-V Measurement System (PV Measurements, Inc.) under simulated illumination of AM 1.5G (100 mW cm⁻²). The devices were measured with non-reflective mask in an ambient atmosphere (device active area: 0.15 cm²). The unencapsulated devices stored under ambient conditions (relative humidity of 60%-80%, room temperature) without illumination was measured every day to evaluate their long-term stability. The continuous illumination stability tests were also performed under AM 1.5G with the relative humidity of 60% at about 40 °C. The external quantum efficiency

(EQE) measurement was carried out by using an internal establishment system with monochromatic light under AM 1.5G illumination. The photodiode used for the calibration of EQE measurements has been calibrated by Newport. Electrochemical impedance spectroscopy measurement was carried out on a Gamry Interface 1000E potentiostat in the frequency range from 1 Hz to 100 KHz in the dark condition, in which the potential bias was fixed at 1.1 V.

ASSOCIATED CONTENT

Supporting Information. XRD patterns, FT-IR spectra, and normalized PL spectra of the pristine and DMEDA₂ treated MAPbI₃ samples; fitted parameters for time resolved PL decay of thin films and devices; TEM and HRTEM images of MAPbI₃ treated by 0.25-DMEDA₂ solution; cross-sectional SEM images of the planar n-i-p PSCs; average photovoltaic parameters and EIS parameters of PSCs.

The following files are available free of charge.

Supporting Information (PDF)

AUTHOR INFORMATION

Corresponding Author

*E-mail: bma@fsu.edu.

Notes

The authors declare no competing financial interest.

ACKNOWLEDGMENT

The authors acknowledge the supports from the National Science Foundation (DMR-1709116), the Air Force Office of Scientific Research (AFOSR) (17RT0906), and the FSU Office of

Research. TEM work was performed at the National High Magnetic Field Laboratory, which is supported by National Science Foundation Cooperative Agreement No. DMR-1644779, and the State of Florida.

REFERENCES

1. Kojima, A.; Teshima, K.; Shirai, Y.; Miyasaka, T., Organometal Halide Perovskites as Visible-Light Sensitizers for Photovoltaic Cells. *J. Am. Chem. Soc.* **2009**, *131*, 6050-6051.
2. Lee, M. M.; Teuscher, J.; Miyasaka, T.; Murakami, T. N.; Snaith, H. J., Efficient Hybrid Solar Cells Based on Meso-Superstructured Organometal Halide Perovskites. *Science* **2012**, *338*, 643-647.
3. Jeon, N. J.; Noh, J. H.; Kim, Y. C.; Yang, W. S.; Ryu, S.; Seok, S. I., Solvent Engineering for High-Performance Inorganic-Organic Hybrid Perovskite Solar Cells. *Nat. Mater.* **2014**, *13*, 897-903.
4. Tsai, H. H.; Nie, W. Y.; Blancon, J. C.; Toumpos, C. C. S.; Asadpour, R.; Harutyunyan, B.; Neukirch, A. J.; Verduzco, R.; Crochet, J. J.; Tretiak, S.; Pedesseau, L.; Even, J.; Alam, M. A.; Gupta, G.; Lou, J.; Ajayan, P. M.; Bedzyk, M. J.; Kanatzidis, M. G.; Mohite, A. D., High-Efficiency Two-Dimensional Ruddlesden-Popper Perovskite Solar Cells. *Nature* **2016**, *536*, 312-316.
5. Jung, E. H.; Jeon, N. J.; Park, E. Y.; Moon, C. S.; Shin, T. J.; Yang, T.-Y.; Noh, J. H.; Seo, J., Efficient, Stable and Scalable Perovskite Solar Cells Using Poly(3-hexylthiophene). *Nature* **2019**, *567*, 511-515.
6. Zhou, C.; Lin, H.; He, Q.; Xu, L.; Worku, M.; Chaaban, M.; Lee, S.; Shi, X.; Du, M.-H.; Ma, B., Low Dimensional Metal Halide Perovskites and Hybrids. *Mater. Sci. Eng. R Rep.* **2019**, *137*, 38-65.

7. Arora, N.; Dar, M. I.; Hinderhofer, A.; Pellet, N.; Schreiber, F.; Zakeeruddin, S. M.; Gratzel, M., Perovskite Solar Cells with CuSCN Hole Extraction Layers Yield Stabilized Efficiencies Greater Than 20%. *Science* **2017**, *358*, 768-771.
8. Wu, F.; Bahrami, B.; Chen, K.; Mabrouk, S.; Pathak, R.; Tong, Y. H.; Li, X. Y.; Zhang, T. S.; Jian, R. H.; Qiao, Q. Q., Bias-Dependent Normal and Inverted J-V Hysteresis in Perovskite Solar Cells. *ACS Appl. Mater. Interfaces* **2018**, *10*, 25604-25613.
9. Jeon, N. J.; Noh, J. H.; Yang, W. S.; Kim, Y. C.; Ryu, S.; Seo, J.; Seok, S. I., Compositional Engineering of Perovskite Materials for High-Performance Solar Cells. *Nature* **2015**, *517*, 476-480.
10. Jiang, Q.; Zhao, Y.; Zhang, X.; Yang, X.; Chen, Y.; Chu, Z.; Ye, Q.; Li, X.; Yin, Z.; You, J., Surface Passivation of Perovskite Film for Efficient Solar Cells. *Nat. Photonics* **2019**, *13*, 460-466.
11. Han, T. H.; Lee, J. W.; Choi, C.; Tan, S.; Lee, C.; Zhao, Y. P.; Dai, Z. H.; De Marco, N.; Lee, S. J.; Bae, S. H.; Yuan, Y. H.; Lee, H. M.; Huang, Y.; Yang, Y., Perovskite-Polymer Composite Cross-Linker Approach for Highly-Stable and Efficient Perovskite Solar Cells. *Nat. Commun.* **2019**, *10*, 520.
12. Zhang, H.; Wu, Y.; Shen, C.; Li, E.; Yan, C.; Zhang, W.; Tian, H.; Han, L.; Zhu, W.-H., Efficient and Stable Chemical Passivation on Perovskite Surface *via* Bidentate Anchoring. *Adv. Energy Mater.* **2019**, *9*, 1803573.
13. Feng, X. X.; Chen, R. H.; Nan, Z. A.; Lv, X. D.; Meng, R. Q.; Cao, J.; Tang, Y., Perfection of Perovskite Grain Boundary Passivation by Eu-Porphyrin Complex for Overall-Stable Perovskite Solar Cells. *Adv. Sci.* **2019**, *6*, 1802040.

14. Grancini, G.; Roldan-Carmona, C.; Zimmermann, I.; Mosconi, E.; Lee, X.; Martineau, D.; Narbey, S.; Oswald, F.; De Angelis, F.; Graetzel, M.; Nazeeruddin, M. K., One-Year Stable Perovskite Solar Cells By 2D/3D Interface Engineering. *Nat. Commun.* **2017**, *8*, 15684.
15. Tan, F.; Tan, H.; Saidaminov, M. I.; Wei, M.; Liu, M.; Mei, A.; Li, P.; Zhang, B.; Tan, C.-S.; Gong, X.; Zhao, Y.; Kirmani, A. R.; Huang, Z.; Fan, J. Z.; Quintero-Bermudez, R.; Kim, J.; Zhao, Y.; Voznyy, O.; Gao, Y.; Zhang, F.; Richter, L. J.; Lu, Z.-H.; Zhang, W.; Sargent, E. H., In Situ Back-Contact Passivation Improves Photovoltage and Fill Factor in Perovskite Solar Cells. *Adv. Mater.* **2019**, *31*, 1807435.
16. Liu, C.; Hu, M. M.; Zhou, X. Y.; Wu, J. C.; Zhang, L. Z.; Kong, W. G.; Li, X. N.; Zhao, X. Z.; Dai, S. Y.; Xu, B. M.; Cheng, C., Efficiency and Stability Enhancement of Perovskite Solar Cells by Introducing CsPbI₃ Quantum Dots as an Interface Engineering Layer. *Npg Asia Materials* **2018**, *10*, 552–561.
17. Zhou, Q.; Liang, L.; Hu, J.; Cao, B.; Yang, L.; Wu, T.; Li, X.; Zhang, B.; Gao, P., High-Performance Perovskite Solar Cells with Enhanced Environmental Stability Based on a (p-FC₆H₄C₂H₄NH₃)₂[PbI₄] Capping Layer. *Adv. Energy Mater.* **2019**, *9*, 1802595.
18. Lin, D.; Zhang, T.; Wang, J.; Long, M.; Xie, F.; Chen, J.; Wu, B.; Shi, T.; Yan, K.; Xie, W.; Liu, P.; Xu, J., Stable and Scalable 3D-2D Planar Heterojunction Perovskite Solar Cells via Vapor Deposition. *Nano Energy* **2019**, *59*, 619-625.
19. Liu, B.; Long, M.; Cai, M.; Ding, L.; Yang, J., Interfacial Charge Behavior Modulation In 2D/3D Perovskite Heterostructure for Potential High-Performance Solar Cells. *Nano Energy* **2019**, *59*, 715-720.

20. Bai, Y.; Xiao, S.; Hu, C.; Zhang, T.; Meng, X. Y.; Lin, H.; Yang, Y. L.; Yang, S. H., Dimensional Engineering of a Graded 3D-2D Halide Perovskite Interface Enables Ultrahigh V_{oc} Enhanced Stability in the p-i-n Photovoltaics. *Adv. Energy Mater.* **2017**, *7*, 1701038.
21. Long, M. Z.; Zhang, T. K.; Chen, D. C.; Qin, M. C.; Chen, Z. F.; Gong, L.; Lu, X. H.; Xie, F. Y.; Xie, W. G.; Chen, J.; Xu, J. B., Interlayer Interaction Enhancement in Ruddlesden-Popper Perovskite Solar Cells toward High Efficiency and Phase Stability. *ACS Energy Lett.* **2019**, *4*, 1025-1033.
22. Zhang, T. Y.; Dar, M. I.; Li, G.; Xu, F.; Guo, N. J.; Gratzel, M.; Zhao, Y. X., Bication Lead Iodide 2D Perovskite Component to Stabilize Inorganic Alpha-CsPbI₃ Perovskite Phase for High-Efficiency Solar Cells. *Sci. Adv.* **2017**, *3*, e1700841.
23. Wen, X. R.; Wu, J. M.; Ye, M. D.; Gao, D.; Lin, C. J., Interface Engineering via an Insulating Polymer for Highly Efficient and Environmentally Stable Perovskite Solar Cells. *Chem. Commun.* **2016**, *52*, 11355-11358.
24. Li, M. H.; Yan, X. Q.; Kang, Z.; Huang, Y. H.; Li, Y.; Zhang, R. X.; Zhang, Y., Hydrophobic Polystyrene Passivation Layer for Simultaneously Improved Efficiency and Stability in Perovskite Solar Cells. *ACS Appl. Mater. Interfaces* **2018**, *10*, 18787-18795.
25. Huang, L. B.; Su, P. Y.; Liu, J. M.; Huang, J. F.; Chen, Y. F.; Qin, S.; Guo, J.; Xu, Y. W.; Su, C. Y., Interface Engineering of Perovskite Solar Cells with Multifunctional Polymer Interlayer Toward Improved Performance and Stability. *J. Power Sources* **2018**, *378*, 483-490.
26. Cai, F. L.; Cai, J. L.; Yang, L. Y.; Li, W.; Gurney, R. S.; Yi, H. N.; Iraqi, A.; Liu, D.; Wang, T., Molecular Engineering of Conjugated Polymers for Efficient Hole Transport and Defect Passivation in Perovskite Solar Cells. *Nano Energy* **2018**, *45*, 28-36.

27. Fairfield, D. J.; Sai, H.; Narayanan, A.; Passarelli, J. V.; Chen, M.; Palasz, J.; Palmer, L. C.; Wasielewski, M. R.; Stupp, S. I., Structure and Chemical Stability in Perovskite-Polymer Hybrid Photovoltaic Materials. *J. Mater. Chem. A* **2019**, *7*, 1687-1699.
28. Abdi-Jalebi, M.; Dar, M. I.; Senanayak, S. P.; Sadhanala, A.; Andaji-Garmaroudi, Z.; Pazos-Outon, L. M.; Richter, J. M.; Pearson, A. J.; Siringhaus, H.; Gratzel, M.; Friend, R. H., Charge Extraction *via* Graded Doping of Hole Transport Layers Gives Highly Luminescent and Stable Metal Halide Perovskite Devices. *Sci. Adv.* **2019**, *5*, eaav2012.
29. Wu, W. Q.; Yang, Z. B.; Rudd, P. N.; Shao, Y. C.; Dai, X. Z.; Wei, H. T.; Zhao, J. J.; Fang, Y. J.; Wang, Q.; Liu, Y.; Deng, Y. H.; Xiao, X.; Feng, Y. X.; Huang, J. S., Bilateral Alkylamine for Suppressing Charge Recombination and Improving Stability in Blade-Coated Perovskite Solar Cells. *Sci. Adv.* **2019**, *5*, eaav8925.
30. Guo, P. F.; Ye, Q.; Yang, X. K.; Zhang, J.; Xu, F.; Shchukin, D.; Wei, B. Q.; Wang, H. Q., Surface and Grain Boundary Co-Passivation by Fluorocarbon Based Bifunctional Molecules for Perovskite Solar Cells with Efficiency Over 21%. *J. Mater. Chem. A* **2019**, *7*, 2497-2506.
31. Zheng, X. P.; Chen, B.; Dai, J.; Fang, Y. J.; Bai, Y.; Lin, Y. Z.; Wei, H. T.; Zeng, X. C.; Huang, J. S., Defect Passivation in Hybrid Perovskite Solar Cells Using Quaternary Ammonium Halide Anions and Cations. *Nat. Energy* **2017**, *2*, 17102.
32. Zhang, Y. Z.; Rong, M. J.; Yan, X. Y.; Wang, X. L.; Chen, Y. L.; Li, X. Y.; Zhu, R. M., Surface Modification of Methylamine Lead Halide Perovskite with Aliphatic Amine Hydroiodide. *Langmuir* **2018**, *34*, 9507-9515.
33. Bu, X. N.; Westbrook, R. J. E.; Lanzetta, L.; Ding, D.; Chotchuangchutchaval, T.; Aristidou, N.; Haque, S. A., Surface Passivation of Perovskite Films *via* Iodide Salt Coatings for Enhanced Stability of Organic Lead Halide Perovskite Solar Cells. *Sol. RRL* **2019**, *3*, 1800282.

34. Wang, Y.; Zhang, T. Y.; Kan, M.; Zhao, Y. X., Bifunctional Stabilization of All-Inorganic alpha-CsPbI₃ Perovskite for 17% Efficiency Photovoltaics. *J. Am. Chem. Soc.* **2018**, *140*, 12345-12348.
35. Li, H.; Tao, L. M.; Huang, F. H.; Sun, Q.; Zhao, X. J.; Han, J. B.; Shen, Y.; Wang, M. K., Enhancing Efficiency of Perovskite Solar Cells via Surface Passivation with Graphene Oxide Interlayer. *ACS Appl. Mater. Interfaces* **2017**, *9*, 38967-38976.
36. Zhang, T. Y.; Hui, Y.; Chen, L.; Li, G.; Mao, B. W.; Zhao, Y. X., Interfacial Crosslinked Quasi-2D Perovskite with Boosted Carrier Transport and Enhanced Stability. *J. Phys. D: Appl. Phys.* **2018**, *51*, 404001.
37. Cho, Y. Y.; Soufiani, A. M.; Yun, J. S.; Kim, J. C.; Lee, D. S.; Seidel, J.; Deng, X. F.; Green, M. A.; Huang, S. J.; Ho-Baillie, A. W. Y., Mixed 3D-2D Passivation Treatment for Mixed-Cation Lead Mixed-Halide Perovskite Solar Cells for Higher Efficiency and Better Stability. *Adv. Energy Mater.* **2018**, *8*, 1703392.
38. Dong, H.; Xi, J.; Zuo, L.; Li, J.; Yang, Y.; Wang, D.; Yu, Y.; Ma, L.; Ran, C.; Gao, W.; Jiao, B.; Xu, J.; Lei, T.; Wei, F.; Yuan, F.; Zhang, L.; Shi, Y.; Hou, X.; Wu, Z., Conjugated Molecules “Bridge”: Functional Ligand toward Highly Efficient and Long-Term Stable Perovskite Solar Cell. *Adv. Funct. Mater.* **2019**, *29*, 1808119.
39. Chen, P.; Bai, Y.; Wang, S. C.; Lyu, M. Q.; Yun, J. H.; Wang, L. Z., In Situ Growth of 2D Perovskite Capping Layer for Stable and Efficient Perovskite Solar Cells. *Adv. Funct. Mater.* **2018**, *28*, 1706923.
40. Cho, K. T.; Grancini, G.; Lee, Y.; Oveisi, E.; Ryu, J.; Almora, O.; Tschumi, M.; Schouwink, P. A.; Seo, G.; Heo, S.; Park, J.; Jang, J.; Paek, S.; Garcia-Belmonte, G.; Nazeeruddin,

M. K., Selective Growth of Layered Perovskites for Stable and Efficient Photovoltaics. *Energy Environ. Sci.* **2018**, *11*, 952-959.

41. Lin, Y.; Bai, Y.; Fang, Y. J.; Chen, Z. L.; Yang, S.; Zheng, X. P.; Tang, S.; Liu, Y.; Zhao, J. J.; Huang, J. S., Enhanced Thermal Stability in Perovskite Solar Cells by Assembling 2D/3D Stacking Structures. *J. Phys. Chem. Lett.* **2018**, *9*, 654-658.

42. Gharibzadeh, S.; Abdollahi Nejang, B.; Jakoby, M.; Abzieher, T.; Hauschild, D.; Moghadamzadeh, S.; Schwenzler, J. A.; Brenner, P.; Schmager, R.; Haghighirad, A. A.; Weinhardt, L.; Lemmer, U.; Richards, B. S.; Howard, I. A.; Paetzold, U. W., Record Open-Circuit Voltage Wide-Bandgap Perovskite Solar Cells Utilizing 2D/3D Perovskite Heterostructure. *Adv. Energy Mater.* **2019**, *9*, 1803699.

43. Mao, L. L.; Ke, W. J.; Pedesseau, L.; Wu, Y. L.; Katan, C.; Even, J.; Wasielewski, M. R.; Stoumpos, C. C.; Kanatzidis, M. G., Hybrid Dion-Jacobson 2D Lead Iodide Perovskites. *J. Am. Chem. Soc.* **2018**, *140*, 3775-3783.

44. Li, Y.; Milic, J. V.; Ummadisingu, A.; Seo, J. Y.; Im, J. H.; Kim, H. S.; Liu, Y. H.; Dar, M. I.; Zakeeruddin, S. M.; Wang, P.; Hagfeldt, A.; Gratzel, M., Bifunctional Organic Spacers for Formamidinium-Based Hybrid Dion-Jacobson Two-Dimensional Perovskite Solar Cells. *Nano Lett.* **2019**, *19*, 150-157.

45. Ahmad, S.; Fu, P.; Yu, S. W.; Yang, Q.; Liu, X.; Wang, X. C.; Wang, X. L.; Guo, X.; Li, C., Dion-Jacobson Phase 2D Layered Perovskites for Solar Cells with Ultrahigh Stability. *Joule* **2019**, *3*, 794-806.

46. Cohen, B. E.; Li, Y. M.; Meng, Q. B.; Etgar, L., Dion-Jacobson Two-Dimensional Perovskite Solar Cells Based on Benzene Dimethan ammonium Cation. *Nano Lett.* **2019**, *19*, 2588-2597.

47. Choi, K.; Lee, J.; Kim, H. I.; Park, C. W.; Kim, G. W.; Choi, H.; Park, S.; Park, S. A.; Park, T., Thermally Stable, Planar Hybrid Perovskite Solar Cells with High Efficiency. *Energy Environ. Sci.* **2018**, *11*, 3238-3247.
48. Peng, W.; Miao, X. H.; Adinolfi, V.; Alarousu, E.; El Tall, O.; Emwas, A. H.; Zhao, C.; Walters, G.; Liu, J. K.; Ouellette, O.; Pan, J.; Murali, B.; Sargent, E. H.; Mohammed, O. F.; Bakr, O. M., Engineering of CH₃NH₃PbI₃ Perovskite Crystals by Alloying Large Organic Cations for Enhanced Thermal Stability and Transport Properties. *Angew. Chem. Int. Ed.* **2016**, *55*, 10686-10690.
49. Cho, K. T.; Paek, S.; Grancini, G.; Roldan-Carmona, C.; Gao, P.; Lee, Y. H.; Nazeeruddin, M. K., Highly Efficient Perovskite Solar Cells with a Compositionally Engineered Perovskite/Hole Transporting Material Interface. *Energy Environ. Sci.* **2017**, *10*, 621-627.
50. Barrit, D.; Cheng, P.; Tang, M.-C.; Wang, K.; Dang, H.; Smilgies, D.-M.; Liu, S.; Anthopoulos, T. D.; Zhao, K.; Amassian, A., Impact of the Solvation State of Lead Iodide on Its Two-Step Conversion to MAPbI₃: An In Situ Investigation. *Adv. Funct. Mater.* **2019**, *29*, 1807544.
51. Li, M. H.; Yeh, H. H.; Chiang, Y. H.; Jeng, U. S.; Su, C. J.; Shiu, H. W.; Hsu, Y. J.; Kosugi, N.; Ohigashi, T.; Chen, Y. A.; Shen, P. S.; Chen, P.; Guo, T. F., Highly Efficient 2D/3D Hybrid Perovskite Solar Cells via Low-Pressure Vapor-Assisted Solution Process. *Adv. Mater.* **2018**, *30*, 1801401.
52. Correa-Baena, J. P.; Luo, Y. Q.; Brenner, T. M.; Snaider, J.; Sun, S. J.; Li, X. Y.; Jensen, M. A.; Hartono, N. T. P.; Nienhaus, L.; Wieghold, S.; Poindexter, J. R.; Wang, S.; Meng, Y. S.; Wang, T.; Lai, B.; Holt, M. V.; Cai, Z. H.; Bawendi, M. G.; Huang, L. B.; Buonassisi, T.; Fenning, D. P., Homogenized Halides and Alkali Cation Segregation in Alloyed Organic-Inorganic Perovskites. *Science* **2019**, *363*, 627-631.

53. Smith, I. C.; Hoke, E. T.; Solis-Ibarra, D.; McGehee, M. D.; Karunadasa, H. I., A Layered Hybrid Perovskite Solar-Cell Absorber with Enhanced Moisture Stability. *Angew. Chem. Int. Ed.* **2014**, *53*, 11232-11235.
54. Ortiz-Cervantes, C.; Carmona-Monroy, P.; Solis-Ibarra, D., Two-Dimensional Halide Perovskites in Solar Cells: 2D or not 2D? *ChemSusChem* **2019**, *12*, 1560-1575.
55. Soe, C. M. M.; Nagabhushana, G. P.; Shivaramaiah, R.; Tsai, H. H.; Nie, W. Y.; Blancon, J. C.; Melkonyan, F.; Cao, D. H.; Traore, B.; Pedesseau, L.; Kepenekian, M.; Katan, C.; Even, J.; Marks, T. J.; Navrotsky, A.; Mohite, A. D.; Stoumpos, C. C.; Kanatzidis, M. G., Structural and Thermodynamic Limits of Layer Thickness in 2D Halide Perovskites. *Proc. Natl. Acad. Sci. U. S. A.* **2019**, *116*, 58-66.
56. Fei, C. B.; Li, B.; Zhang, R.; Fu, H. Y.; Tian, J. J.; Cao, G. Z., Highly Efficient and Stable Perovskite Solar Cells Based on Monolithically Grained $\text{CH}_3\text{NH}_3\text{PbI}_3$ Film. *Adv. Energy Mater.* **2017**, *7*, 1602017.
57. Abdelmageed, G.; Mackeen, C.; Hellier, K.; Jewell, L.; Seymour, L.; Tingwald, M.; Bridges, F.; Zhang, J. Z.; Carter, S., Effect of Temperature on Light Induced Degradation in Methylammonium Lead Iodide Perovskite Thin Films and Solar Cells. *Sol. Energ. Mat. Sol. C.* **2018**, *174*, 566-571.
58. Huang, W. X.; Wang, Y. X.; Balakrishnan, S. K., Controllable Transformation Between 3D and 2D Perovskites Through Cation Exchange. *Chem. Commun.* **2018**, *54*, 7944-7947.
59. Huang, W. X.; Sadhu, S.; Sapkota, P.; Ptasinska, S., In Situ Identification of Cation-Exchange-Induced Reversible Transformations of 3D and 2D Perovskites. *Chem. Commun.* **2018**, *54*, 5879-5882.

60. Lee, J. W.; Dai, Z. H.; Han, T. H.; Choi, C.; Chang, S. Y.; Lee, S. J.; De Marco, N.; Zhao, H. X.; Sun, P. Y.; Huang, Y.; Yang, Y., 2D Perovskite Stabilized Phase-Pure Formamidinium Perovskite Solar Cells. *Nat. Commun.* **2018**, *9*, 3021.
61. Yuan, S.; Qian, F.; Yang, S.; Cai, Y.; Wang, Q.; Sun, J.; Liu, Z.; Liu, S., NbF₅: A Novel α -Phase Stabilizer for FA-Based Perovskite Solar Cells with High Efficiency. *Adv. Funct. Mater.* **2019**, *29*, 1807850.
62. Tavakoli, M. M.; Saliba, M.; Yadav, P.; Holzhey, P.; Hagfeldt, A.; Zakeeruddin, S. M.; Gratzel, M., Synergistic Crystal and Interface Engineering for Efficient and Stable Perovskite Photovoltaics. *Adv. Energy Mater.* **2019**, *9*, 1802646.
63. Meng, L.; Sun, C. K.; Wang, R.; Huang, W. C.; Zhao, Z. P.; Sun, P. Y.; Huang, T. Y.; Xue, J. J.; Lee, J. W.; Zhu, C. H.; Huang, Y.; Li, Y. F.; Yang, Y., Tailored Phase Conversion under Conjugated Polymer Enables Thermally Stable Perovskite Solar Cells with Efficiency Exceeding 21%. *J. Am. Chem. Soc.* **2018**, *140*, 17255-17262.
64. Gao, L.; Spanopoulos, I.; Ke, W.; Huang, S.; Hadar, I.; Chen, L.; Li, X.; Yang, G.; Kanatzidis, M. G., Improved Environmental Stability and Solar Cell Efficiency of (MA,FA)PbI₃ Perovskite Using a Wide-Band-Gap 1D Thiazolium Lead Iodide Capping Layer Strategy. *ACS Energy Lett.* **2019**, *4*, 1763-1769.
65. Tai, Q. D.; You, P.; Sang, H. Q.; Liu, Z. K.; Hu, C. L.; Chan, H. L. W.; Yan, F., Efficient and Stable Perovskite Solar Cells Prepared in Ambient Air Irrespective of the Humidity. *Nat. Commun.* **2016**, *7*, 11105.
66. Zhao, H.; Wang, S. R.; Sun, M. N.; Zhang, F.; Li, X. G.; Xiao, Y., Enhanced Stability and Optoelectronic Properties of MAPbI₃ Films by a Cationic Surface-Active Agent for Perovskite Solar Cells. *J. Mater. Chem. A* **2018**, *6*, 10825-10834.

67. Yang, G.; Chen, C.; Yao, F.; Chen, Z.; Zhang, Q.; Zheng, X.; Ma, J.; Lei, H.; Qin, P.; Xiong, L.; Ke, W.; Li, G.; Yan, Y.; Fang, G., Effective Carrier-Concentration Tuning of SnO₂ Quantum Dot Electron-Selective Layers for High-Performance Planar Perovskite Solar Cells. *Adv. Mater.* **2018**, *30*, 1706023.
68. Saliba, M.; Correa-Baena, J. P.; Wolff, C. M.; Stolterfoht, M.; Phung, N.; Albrecht, S.; Neher, D.; Abate, A., How to Make over 20% Efficient Perovskite Solar Cells in Regular (n-i-p) and Inverted (p-i-n) Architectures. *Chem. Mater.* **2018**, *30*, 4193-4201.

Table of Contents

